Semiconductors, Vol. 34, No. 11, 2000, pp. 1229–1247. Translated from Fizika i Tekhnika Poluprovodnikov, Vol. 34, No. 11, 2000, pp. 1281–1299.

REVIEWS

Silicon–Germanium Nanostructures with Quantum Dots: Formation Mechanisms and Electrical Properties

O. P. Pchelyakov*, Yu. B. Bolkhovityanov*, A. V. Dvurechenskiĭ*, L. V. Sokolov*, A. I. Nikiforov*, A. I. Yakimov*, and B. Voigtländer**

** Institute of Semiconductor Physics, Siberian Division, Russian Academy of Sciences, pr. Akademika Lavrent'eva 13, Novosibirsk, 630090 Russia*

*** Research Center, Yuelich, Germany*

Submitted April 17, 2000; accepted for publication May 10, 2000

Abstract—The generally accepted notions about the formation mechanisms for germanium islands with nanometer-scale sizes in a Ge-on-Si system are reviewed on the basis of analysis of recent publications. The presence of elastic strains in the epilayers and in the three-dimensional Ge islands on Si is a key factor that not only initiates a morphological transition from a planar film to an island-containing film (the Stranski–Krastanov mechanism) but also influences the subsequent stages of the islands' evolution, including their shape, size, and spatial distribution. In many cases, this factor modifies appreciably the classical mechanisms of phase-formation and their sequence up to the quasi-equilibrium coexistence of three-dimensional Ge nanoislands at the surface of the Si substrate. The methods for improving the degree of the ordering of nanoislands to attain the smallest possible sizes and large density of areal distribution of these islands are discussed. The published data on optical absorption in the multilayered Ge–Si systems with quantum dots are considered; these data are indicative of an anomalously large cross section of intraband absorption, which makes this class of nanostructures promising for the development of photodetectors of the infrared region of the spectrum. The results of original studies of electrical and optical properties of heterostructures that involve Ge quantum dots and are synthesized by molecular-beam epitaxy on the Si substrates are reported. © *2000 MAIK "Nauka/Interperiodica".*

1. INTRODUCTION

Nanostructures based on the germanium-on-silicon heterosystem attract the attention of technologists owing to significant progress in the development of new quantum-effect devices in spite of a 4% difference between the lattice parameters of Ge and Si. We witness the appearance of silicon–germanium light-emitting and photodetecting devices that make silicon technology quite competitive with those of conventional optoelectronic materials, such as the III–V compounds [1–5]. In recent years, the potential applications of the Ge–Si-based semiconductor materials containing the nanometer-sized Ge clusters (quantum dots) embedded in the Si matrix have become apparent. Interest in the Ge and Si nanoclusters is related to the following circumstances: (i) progress in the development of technology for producing a Ge-nanocluster array that is fairly uniform in size; (ii) the sizes of nanoclusters have been reduced to the values that ensure the manifestation of the size-quantization effects and the electron–electron interaction up to room temperature; and (iii) compatibility of the developed methods with existing silicon technology for the production of discrete devices and circuits. Such designs that have been considered exotic until recently may bring about an actual revolution in silicon integration technology.

A steady increase in the number of publications worldwide devoted to low-dimensional heterostructures is indicative of the growing interest in these structures. Figure 1 shows the histograms for the number of annual publications that include the keywords "quantum wells" and "quantum dots." In the latter case, a steady increase in the annual number of relevant publications is observed. Starting in 1992, changes became evident in the technology producing the structures with quantum dots. Before that time, the main method for forming such structures was photolithography, with the constraint on the minimum sizes inherent in this method. Manifestation of the effect of ordering in the array of nanometer-sized islands in the Ge–Si and InAs–GaAs heterosystems made it possible to obtain quantum dots that had no defects, had the smallest possible size (10–100 nm), and had the density of 10^{10}–10^{11} cm^{-2}, which made the atomlike characteristics of these systems more pronounced in the relevant electronic and optical spectra. The development of studies in this field is illustrated in Fig. 2 by histograms of the annual number of publications devoted to a Ge–Si system. It is in this system that the arrays of islands were first used to observe the one-electron effects [6]. Later, most studies of electronic properties of quantum dots (QDs) were based on III–V compounds. This was caused by the following factors: (a) progress in the technology of heteroepitaxy for III–V compounds; (b) the possibility of producing the heterostructures of type I (the offsets of the conduction

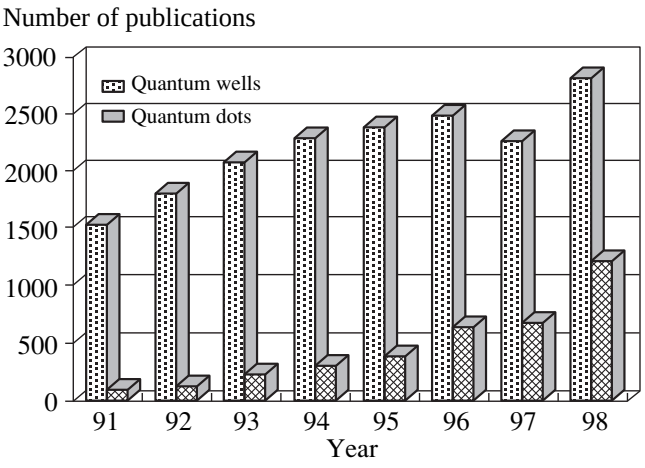

Fig. 1. The number of annual publications according to the data of the Materials Science Citation Index (MSCI) for 1990–1998. Search was based on the keywords "quantum wells" and "quantum dots."

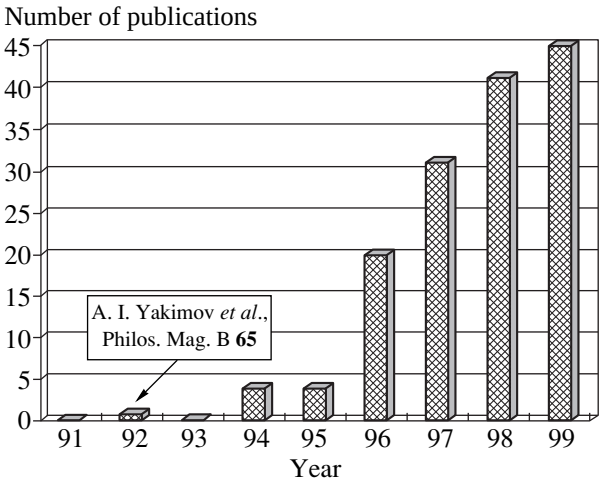

Fig. 2. Selection (from the complex "quantum dots," see Fig. 1) of publications devoted to the island growth of Ge (GeSi) on Si and also to the properties of these entities (for the year 1999, the data are given for 10 months; the data refer to the most important journals).

and valence bands are of opposite signs), which is important for the optical properties of these systems; and (c) the small value of the charge-carrier effective mass, which ensured the manifestation of size-quantization effects for islands of a relatively large size. The first studies of QDs in III–V compounds were performed on the basis of InAs–GaAs structures [7, 8].

A transition from the layer-by-layer [i.e., two-dimensional (2D)] growth of the film to the formation of three-dimensional (3D) islands (the Stranski–Krastanov mechanism) has been studied for a long time in the germanium-on-silicon heterosystem. The first publication devoted to this heterosystem, in which the observation of pseudomorphous Ge stripes (referred to now as quantum wires) that follow the outlines of steps and of the nanometer-sized islands (currently, quantum dots) was reported, was apparently that of the study [9] performed at the Institute of Semiconductor Physics (Siberian Division, Academy of Sciences of USSR) as far back as 1974. At relatively low temperatures of synthesis, such islands do not contain the misfit dislocations even if the thickness of the islands exceeds appreciably the critical value, which was demonstrated most clearly in studies of the Ge–Si [10] and InGaAs–GaAs [11] systems. Following these publications, a sharp increase in the study of the mechanisms of formation of strained islands and the special features of their ordering set in, because an opportunity arose to form 3D objects that have no defects (no misfit dislocations), have nanometer-scale sizes, and may find practical applications in nanoelectronics.

The objective of this review was to analyze the development and current ideas about the mechanisms of ordering of the QD ensembles in the course of heteroepitaxy. This has been the subject of a number of reviews [12–14]. However, without laying claim to completeness, as concerns a review of all heterosystems, we have attempted to outline the generally accepted concepts of the Ge-on-Si system and to supplement these with an analysis of the newest data, including the results of our experiments with synthesis of a Ge–Si heterosystem with QDs, and the study of the electronic and optical properties of this heterosystem.

In Section 2, we consider the driving forces and main mechanisms of evolution and ordering of nanoobjects in heterosystems with a large lattice mismatch in the course of molecular-beam epitaxy (MBE) and heat treatment. In Section 3, we analyze the experimental observations of cluster formation and self-organization for Ge–Si nanostructures at the silicon surface and discuss the feasible methods for enhancing the ordering, reducing the sizes, and increasing the density of the germanium QDs. In Section 4, we summarize the original results of our studies of the electronic and optical properties of heterostructures and multilayered compositions with Ge QDs.

2. BASIC PREMISES

It is possible to distinguish between the stages of nucleation and further development in the formation of 3D islands. The main pattern in the nucleation of islands in an epitaxial heterosystem is governed by the balance between the surface energies of the film and substrate and also between the energy of the film–substrate interface and internal energy of the island bulk. The free energy of a newly formed island nucleus at the substrate surface may be expressed as the sum of three terms [15]; i.e.,

$$\Delta G = -V\Delta\mu + \gamma s + E_i(V, h/l).$$

Here, the first term accounts for the formation energy of a new nucleus with the volume V, with $\Delta\mu$ standing for the thermodynamic force for crystallization in the event of supersaturation. The second term corresponds to the work required for the formation of additional surface area s, with γ standing for the nucleus surface energy. The third term describes additional energy that is brought about owing to elastic strain in the nucleus. The first and second terms in the above expression correspond to the classical version of the nucleation theory (see, for example, [16]), whereas the third term appears only in the case where strained films are grown. For large values of the lattice mismatch, such as those that occur in a Ge–Si system, this additional energy depends not only on the nucleus volume, but also on its shape (i.e., on the ratio h/l, where h is the height and l is the cross-sectional dimension of the nucleus), and is important in the transition from the 2D to 3D growth mechanisms. According to calculations [15], the contribution of this term is represented by a rapidly decreasing function of h/l. The more pronounced the 3D state of a strained nucleus, the larger the contribution of elastic relaxation (a decrease in the strain in the regions of the nucleus that are the most remote from the substrate), and the smaller the additional contribution of the strain energy to the free energy of the nucleus. The surface energy of a system composed of the Ge film (with Ge island) and the Si substrate also depends on the Ge coating thickness (and the shape of the Ge island) [15, 17]. At present, it is generally believed that the key factor in the transition from the 2D (layer-by-layer) to the 3D (island-type) growth of pseudomorphous films is an energy gain due to a decrease in elastic stresses via their elastic relaxation. We note that, in the case of homoepitaxy on a fairly clean surface, the bulk islands are not formed for almost all semiconductors, and the film grows owing to either the motion of step (the step–layer growth) or the formation and coalescence of 2D islands. As will be clear from what follows, stresses also play an important role in the development of 3D islands and their distribution in size.

The determining role of elastic relaxation, which brings about the morphological instability of the film surface, was demonstrated by Asaro and Tiller (1972) [18] and by Grinfel'd (1986) [19]. The basic aspect of this model is the proposition that the rough surface of a strained layer has a lower total energy (the strain energy combined with the surface energy) as a result of elastic relaxation of stresses at the tops of asperities. An increase in the surface energy due to an increase in the rough-surface area is a factor that opposes the development of the film's surface relief; however, this factor reduces the energy gain via relaxation only in part [19]. The larger the mismatch between the film and substrate lattices, the smaller the thickness of the pseudomorphous film at which morphological stability is lost. The formation of islands is an extreme manifestation of morphological instability of strained films and is commonly observed in systems with large values of mismatch between the film and substrate lattices ($\varepsilon > 2\%$); the Ge–Si and InAs–GaAs structures are typical representatives of such systems. If the surface energy of a new phase is somehow reduced, the strained film can lose its morphological stability even for small values of mismatch. Thus, if the strained film is in contact with a liquid phase, in which case the surface energy of the film is appreciably lower than that of the film–vacuum (or film–vapor) interface, formation of islands is observed in a Ge_xSi_{1-x}–Si(001) system for low values of the mismatch $x \approx 0.05$ ($\varepsilon \approx 0.2\%$) [20]. The same small values of elastic strains brought about a branching in the shape of the island-type film in an $In_xGa_{1-x}As$–GaAs(111)*A* system formed also in contact with a liquid phase, and the splitting of this system into separate micrometer-sized islands [21]. In this paper, a a unique example of observing the dislocation-free islands that are formed on the substrate with (111) orientation and have a thickness exceeding the critical value for the introduction of misfit dislocations is reported; apparently, this result is a consequence of a decrease in the surface energy of the film that is in contact with the liquid phase.

According to classical notions (see, for example, [22]), formation of a new phase includes the following main stages: nucleation of the new-phase centers, their independent growth, and, finally, the development of these centers in interaction with each other (the so-called Ostwald ripening). This phenomenon represents the latest stage of evolution of the new-phase nuclei. If the objective of the study consists in producing an island-type film (as in the case under consideration), this stage of the Ostwald ripening may happen to be the main stage that defines the shape of the island distribution by size. Therefore, the applicability of the Ostwald-ripening model to the analysis of the self-organization of quantum-dimensional clusters in a Ge–Si system (and other systems) has received much attention in available publications.

The first comprehensive theory of Ostwald ripening to describe the formation of clusters (grains) in a volume of supersaturated solid solutions was developed by Lifshitz and Slyozov [23]. Later, this theory was modified by Chakraverty [24] so as to be applied to the surface. Recently, this theory has been widely used to interpret the processes observed at the semiconductor surface using modern high-resolution methods (see, for example, [25–29]). According to this model, the later stage in the development (ripening) of clusters is governed by the interaction of nuclei found within a saturated "sea" of adatoms via the Gibbs–Thomson effect (the equilibrium vapor pressure above the curvilinear surface of the nucleus should be higher than in other cases). The small-sized islands decrease in size owing to a more pronounced curvilinearity of the surface (or the pedestal of a cluster) and, ultimately, cease to exist, whereas the large islands grow. A characteristic feature of the Ostwald-ripening mechanism is a continuous

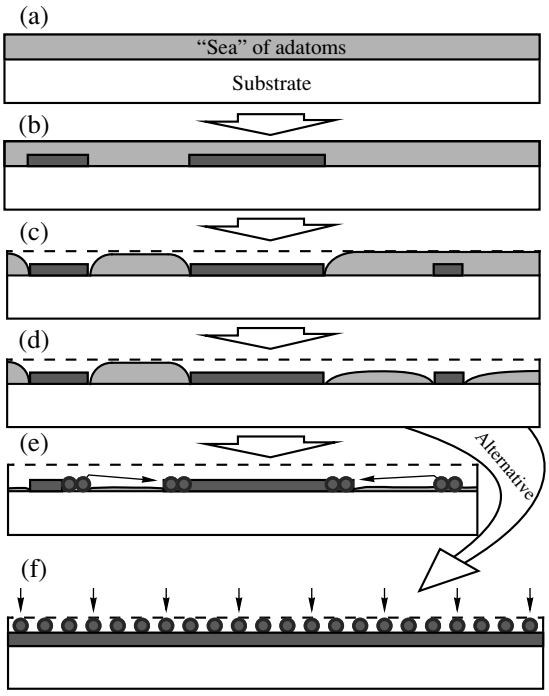

Fig. 3. Schematic representation of the initiation and formation of a new monolayer according to classical concepts forwarded by Kukushkin and Osipov [22] as applied to molecular epitaxy (for example, epitaxy of silicon on silicon). For details, see the text.

increase in the average island size with time and a broadening of the unnormalized distribution of islands in size.

Experimental observations of the development of 2D Si islands at the Si(100) surface are in close agreement with inferences from the Ostwald-ripening model (see, for example, [26]). Figure 3 illustrates schematically the formation and development of a new epitaxial monolayer according to classical concepts of the three stages [22]. In the initial state (representation a), there is a supersaturated adsorbate of Si atoms (a "sea" of adatoms) at the substrate surface, and, in the first stage, nucleation of 2D centers occurs (representation b). Following this comes the second stage consisting in the independent growth of the centers (representation c). During this stage, supersaturation around the centers is reduced; however, these centers do not yet interact with each other because their diffusion-source "feeding" fields do not yet overlap. Therefore, nucleation of new centers continues at the sites away from the islands that have been already formed (representation c, the center at the right). After the diffusion-source fields have overlapped (representation d) and the supersaturation between the islands has been reduced even more, there comes the third stage that consists in the correlated growth of the islands or the Ostwald ripening. According to Kukushkin and Osipov [22], the interaction between the islands occurs via a "generalized self-consistent diffusion-source field" (in the case under consideration, this field is represented by the Si adsorbate). Large islands grow, whereas the small islands cease to exist (representation e). This stage may span a long time if the system is closed and the number of adatoms amounts to less than a single monolayer [26]. The island-size distribution is a reproducible function that depends appreciably on the substrate orientation (see, for example, [30]). In the case of a continuous supply of atoms to the surface (an open system), the islands grow until they are in contact with each other; thus, a continuous monolayer is formed (representation f).

Lifshitz and Slyozov studied the ripening of grains and stated [23], in particular, that elastic strains in the grains may be taken into account, although this would not appreciably affect the shape of the final distributions, because the strains constitute a second-order correction. In fact, in the 3D case considered by Lifshitz and Slyozov, the strains in the 3D grains of a new material may be treated as an addition to the free energy of a cluster; this addition affects the nucleation and the growth rates of the cluster. Such an approach was used by Drucker [31] to evaluate the development of 2D islands at the substrate surface in the case of the Ostwald ripening. However, recent studies have shown that elastic strains in epitaxial films and nucleating 3D islands constitute a key and a multivalued factor that, in the majority of cases, changes radically the pattern of the classical phase-formation mechanisms. Thus, for the growth of Ge on Si and InAs on GaAs, it is the presence of these strains that induces the transition from layer-by-layer growth to the formation of 3D clusters at the surface of underlying Ge (or InAs) layer; as a result, the Stranski–Krastanov mechanism comes into effect. Significant nonuniformity of the elastic relaxation of an island over its height causes the energy gain to depend on the island shape. Several discrete shapes that are most favorable energetically (a "hut,", a "dome," and a "superdome") come into existence. Elastic strains at the cluster periphery increase with increasing cluster size, which affects the rules of attachment of adatoms to a cluster; as a result the growth rate of the clusters decreases [32–34]. It is believed that the emergence and heightening of the barrier related to the above constitute one of the main causes of the observation that the island-size distribution is narrower compared to theoretical predictions based on the Ostwald ripening (see, for example, [33]). Under certain conditions, the role of elastic strains and their relaxation in the islands becomes dominant until a quasi-equilibrium state is established. In this state, both the shape and the size-distribution of islands is time-independent; correspondingly, the ensemble of islands cannot be described in the context of the model based on the Ostwald ripening [29, 35–40].

Figure 4 illustrates schematically the main stages of formation of the strained-island ensemble and their difference from the classical variant. Similarly to what was shown in Fig. 3, there is initially a supersaturated

adsorbate at the surface (a); however, this adsorbate is now formed at the surface of underlying (wetting) layer from the deposited material (Ge). Nucleation of the 3D hut-shaped clusters (representation b) is caused by the elastic-strain relaxation (this is the first difference from the classical theory). Later (representation c), two distinct shapes ("hut" and "dome") come into existence. The energetic advantages of the first and second shapes depends on their volume; however, under certain conditions, the coexistence of these shapes is possible [35, 36] (the second difference from the classical theory). The flow of atoms to the islands with shapes that are more energetically favorable was observed [41] (representation d). In this case, the model of the Ostwald ripening is apparently valid (small islands cease to exist, and large islands grow); however, the island-size distribution is now bimodal rather than unimodal [36, 41]. A reverse transition from a dome shape to a hut shape was also observed (the third difference from the classical theory) [38, 40, 42]. A quasi-equilibrium state of the system is possible, in which case the sizes and shapes of the clusters are virtually time-independent if there is no external flux [39] (representation e) (the fourth difference from classical theory). Chiu [43] has demonstrated theoretically that the probability of the state of the ensemble being stable increases with increasing surface-energy anisotropy (as this energy increases at the facets of the islands). Under certain conditions (when the islands are closely spaced), the interaction of clusters via overlapping elastic-deformation fields in the substrate was substantiated theoretically [44, 45]; this interaction may be conducive to the ordering of spatial distribution of islands at the surface (the fifth difference from the classical theory). Consideration of elastic interaction via the substrate in a system of GeSi–on–Si islands made it possible to interpret the experimental results [46] correctly.

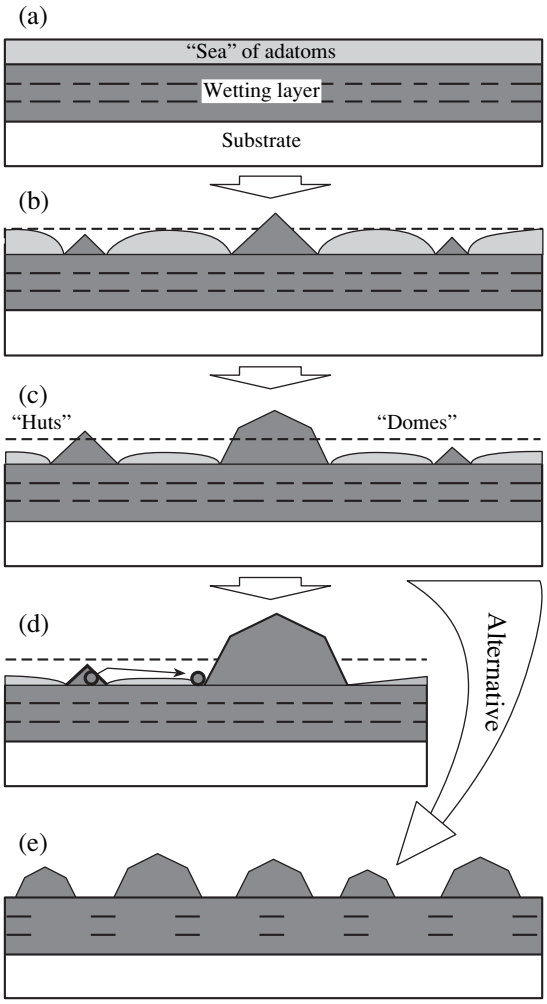

Fig. 4. Schematic representation of the stages of formation of three-dimensional islands in a Ge–Si(001) system. For details, see the text.

3. GROWTH AND SPECIAL FEATURES OF ORDERING IN THE ENSEMBLES OF Ge NANOCLUSTERS

3.1. Morphological Reconstructions

Several stages of the island evolution are observed experimentally in the Ge–Si systems. These stages differ for the substrates with (001) and (111) orientations. From the standpoint of producing quantum objects, the (001) surface is unique, because the compact 3D dislocation-free islands 10–100 nm in size were observed at this surface alone (Fig. 5). Emergence of such islands is observed after a continuous Ge film has been formed; the superstructure domains in this film are easily distinguished between the islands in Fig. 5. The onset of formation of the 3D clusters is accompanied by the emergence of strands in the patterns of high-energy electron diffraction (HEED); these strands are formed as a result of electron scattering by the {105} faces. Such islands are referred to as hut-clusters due to their shape [47]. As the average film thickness increases, the HEED patterns indicate the presence of {113} and {102} faces in addition to the {105} faces. It should be noted that the first study where the HEED method was used to reveal these faces of the Ge islands at the Si(001) surface was carried out the Institute of Semiconductor Physics (Siberian Division, Academy of Sciences of the USSR) as far back as 1987 [48]. The formation of the dome-shaped clusters is characteristic of this stage of growth. A transition from the hut-shaped clusters with sizes of 15–20 nm at the pedestal of the dome-shaped clusters (with average sizes of 50–100 nm) is accompanied with an increase in the degree of relaxation of stresses. According to the data obtained by Floro *et al.* [49], the material in the hut-shaped clusters is elastically relaxed by 20% on average, whereas in the dome-shaped clusters, the relaxation amounts to more than 50% due to a larger ratio between the height and the pedestal size; in this case, the islands remain coherently matched to the substrate. As follows from numerous experimental observations, the last stage in the development and

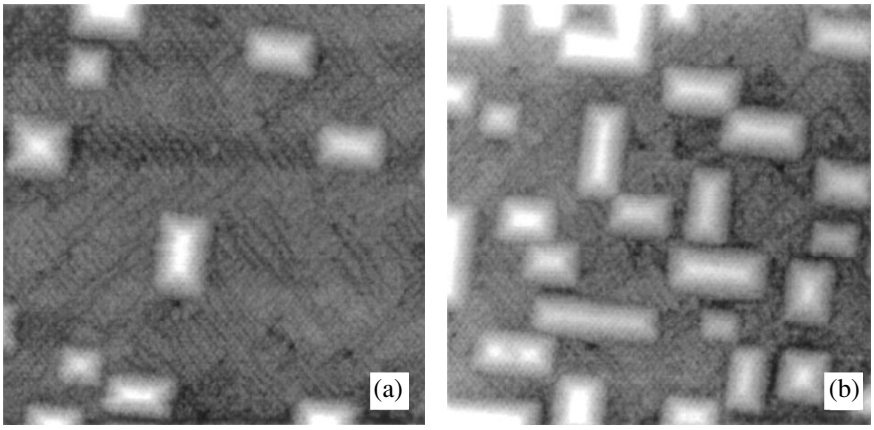

Fig. 5. An STM image of hut-shaped clusters on the Si(001) surface covered with a Ge sublayer with a thickness d_{eff} = (a) 4.6 and (b) 8 ML; T_g = 300°C. The side of the image amounts to 160 nm. STM stands for scanning tunneling microscopy.

structure of Ge_xSi_{1-x} islands on Si(001) and Si(111) consists in the formation of 3D plastically strained islands with misfit dislocations at the interface with the substrate, which is accompanied with a rapid increase in the island sizes (see, for example, [50–52]).

3.2. The Effects of Ordering

Ordering brings about the emergence of islands with preferential sizes, shapes, interisland distances, and relative positions in the system. This is a result of the minimization of the total free energy of the system. The existence of preferential characteristics should manifest itself in the scattering and diffraction spectra of electrons and X-rays interacting with the surface that contains the nanostructures and also in the electronic and optical spectra.

The distribution of Ge islands in size is given much attention in various publications because this parameter of the QD system is extremely important for practical applications. Typical island-size distributions and the range of normalized rms deviations $\sigma/\langle l\rangle$ ($\langle l\rangle$ is the average size) that define the broadening of the distributions are shown schematically in Fig. 6. According to the data reported elsewhere [29], narrower distributions are observed for the dome-shaped islands with average sizes of 50–100 nm (in [29], the Ge islands were grown by chemical deposition in an atmosphere of hydrogen that affects the mobility of Ge adatoms). The narrower distributions for the dome-shaped cluster are explained by the fact that an increase in elastic strain in the substrate, and in the cluster pedestal as the cluster size increases, reduces the growth rate of the cluster (in contrast with cluster development according to the mechanism of the Ostwald ripening). For the hut-shaped clusters obtained by the MBE [34], a similar pattern was observed; i.e., the growth rate of a hut-shaped Ge cluster decreased as its size increased (this phenomenon was studied in more detail in [34]). The above brings about an appreciable narrowing of the island-size distribution. An estimation of the broadening of the distributions for the Ge hut-shaped clusters (shown in Fig. 5) yields $\sigma/\langle l\rangle \sim 0.2$–$0.25$, which is appreciably smaller than for the hut-shaped clusters grown in the hydrogen atmosphere [29] (see Fig. 6, curve *a*). The most uniform Ge island-size distribution was reported in [53] ($\sigma/\langle l\rangle = 0.032$), and, with permission granted by the authors, such islands are shown in Fig. 7a. Such a narrow distribution, was obtained (according to the authors of [53]) owing to a thorough selection of the growth conditions.

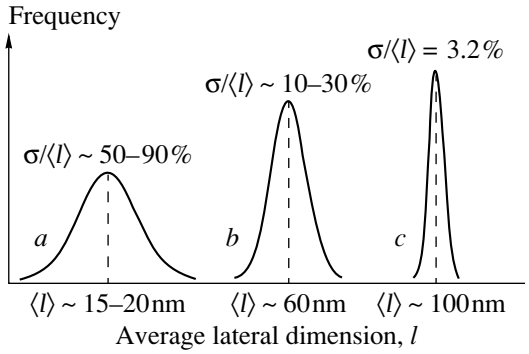

Fig. 6. Characteristic rms deviations ($\sigma/\langle l\rangle$) of the island sizes in a Ge–Si system: (*a*) for the hut-shaped islands, (*b*) for the dome-shaped islands (according to [29]); and (*c*) the distribution obtained by Jiang and coworkers [53]. The distributions are shown schematically.

The other following methods for enhancing the uniformity of the island sizes should be mentioned: (i) the use of tilted substrates, and (ii) the use of a special method for ensuring the simultaneous nucleation of the clusters [54]. The substantiation of these methods can be found in the following known facts and reasoning. In the publication by Goldfarb *et al.* [27], the details of transition from 2D to 3D growth and the initial stages of formation of the hut-shaped clusters were elaborated. The 3D islands appear at significantly different

points in time and are nucleated at imperfections of the 2D Ge layer, which confirms the generally accepted opinion that cluster nucleation is heterogeneous. Consequently, the preliminary formation of the sites that are preferential for the cluster nucleation may constitute a useful method for enhancing the ordering of these clusters. A preliminary ordering of steps at the surfaces that are disoriented with respect to (001) is widely used to form the QD arrays in an InAs–GaAs system (see, for example, one of the latest publications by Kim *et al.* [55] and the references therein). In the case of growing the Ge islands on Si, such an approach is used to a lesser extent; however, in order to enhance the ordering of steps at the 2D stage of growth, the authors of [56] not only used the steps' ordering related to the deviation of the substrate from the singular direction but also improved this ordering by preliminary overgrowth of the multilayered strained GeSi–Si superlattice. As a result [56], Ge islands having a uniformity of distribution both in height and in area of better than 10% with simultaneous significant spatial ordering were obtained (Fig. 7b).

According to the data obtained by Johansson and Seifert [57], the width of the island-size distribution (for InAs/InP) depends nonmonotonically on the growth rate. The distribution width decreases with increasing growth rate and reaches a minimum. As the growth rate increases further, the distribution broadens again. Such behavior verifies the importance of a single-moment heterogeneous nucleation. As the growth rate increases, the probability of the island nucleation at the onset of the process becomes higher; as a result, the islands grow for the same length of time and have almost the same dimensions. A further increase in the growth rate gives rise to the adatom supersaturation at the surface becoming so high that new islands are nucleated continuously. Because of this, the instant of nucleation again becomes spread, and the island-size distribution broadens.

It is possible to ensure an almost simultaneous nucleation of islands over the entire surface area of the substrate by providing an appreciable supersaturation of germanium adatoms at the initial instant of growth. This can be ensured, for example, by a short-term increase in the molecular-beam density or by a short-term decrease in the substrate temperature. The effect of synchronizing periodic short-term variations in the surface supersaturation on the 2D nucleation was observed by us previously in the case of homoepitaxy of silicon and germanium. On the basis of this effect, the MBE method with synchronization of nucleation was substantiated and implemented [54]. Later, an optimized method for the synthesis of quantum-dimensional structures such as the vertical superlattices, nanosystems consisting of quantum wires or dots, and the like, was suggested and substantiated theoretically for cyclic variation of supersaturation during the growth of each atomic layer of the film [58].

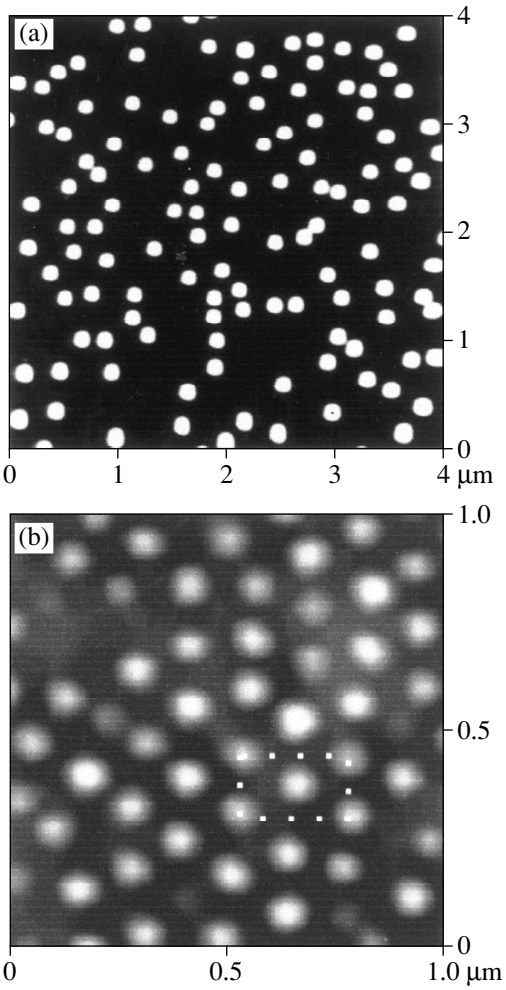

Fig. 7. Ge islands at the Si surface: (a) at a singular Si(001) face with the growth conditions specially selected (with permission given by the authors of [53]) and (b) at a vicinal Si(001) face with a preliminarily grown GeSi/Si superlattice [56] (with permission given by the authors of [56]).

Ordering with respect to the area is the weakest form of ordering, which is related to the fact that the islands interact weakly with each other at the initial stage of their formation. Therefore, the preliminary formation of ordered sites for the nucleation of nanoclusters is the most important method for ensuring their subsequent spatially ordered state. This statement is confirmed by an analysis of the two distributions of Ge islands over the singular (Fig. 7a) and vicinal (Fig. 7b) (100) Si faces. Figure 8 shows the spatial-ordering characteristics obtained by statistically processing the data shown in Fig. 7: the radial correlation functions that define the probability of finding the cluster at a certain distance from an arbitrarily chosen island (Figs. 8a, 8b). It can be seen that, in spite of an extremely small scatter in the parameters of the islands [53] whose microphotographs are shown in Fig.7a, their spatial distribution is almost unordered. A certain degree of

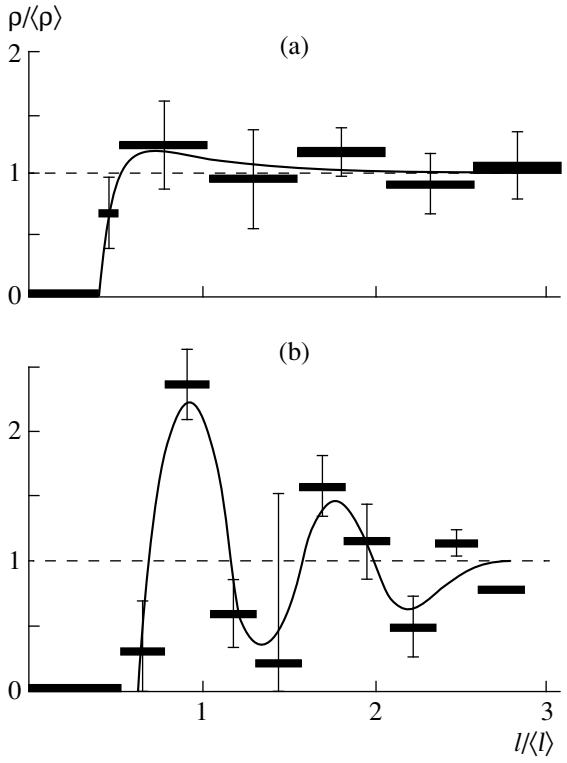

Fig. 8. Radial distributions of the normalized density of islands as a function of the normalized distance from an arbitrarily chosen particle for the above microphotographs (Figs. 8a and 8b correspond to Figs. 7a and 7b).

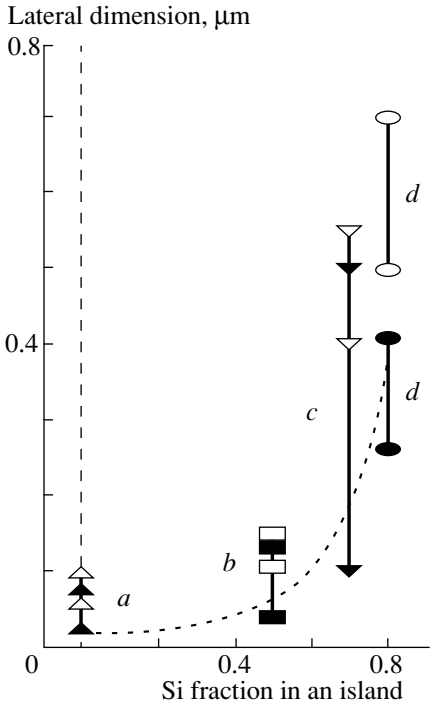

Fig. 9. Schematic representation of variations in the sizes of the hut- and dome-shaped clusters with increasing silicon fraction in an island on the basis of publications by (*a*) Kamins *et al.*, (*b*) Vostokov *et al.* [42], (*c*) Ross *et al.* [63], and (*d*) Floro *et al.* [49]. The dotted line represents the calculated waviness of the surface of a strained GeSi solid solution according to Obayashi and Shintani [64].

ordering is evidenced by the presence of a poorly pronounced preferential distance between the nearest neighbors and by the absence of 3D centers spaced at smaller than average intervals (Fig. 8a). Spatial distribution of the islands shown in Fig. 7b [56] may be considered as the most ordered among those observed in the Ge–Si system. The form of the correlation function shown in Fig. 8b is indicative of the presence of the short-range order in the first and second coordination shells. Spatial ordering of the islands becomes more pronounced with increasing coverage (the ratio between the total area of the islands and the substrate area), which is caused by minimization of repulsive forces of elastic interaction between neighboring islands [46, 59]. Because of this, the most highly spatially ordered arrays of islands occupy the largest fraction of the substrate area (see, for example, Fig. 7b, where the islands are nearly in contact with each other).

It was shown previously [13] that the sequential growth of layers with Ge islands overgrown with a material that is lattice-matched to the substrate (Si) causes the ordering (with respect both to the sizes and areas) to become more pronounced. The elastic-deformation fields are perturbed by clusters; these perturbations penetrate into the overgrown layer to different depths, depending on the volume of a specific island and on the degree of the island accumulation. The sites of preferential nucleation of new islands at the next level are formed at the surface of the overgrown layer. By varying the overgrown-layer thickness, one can suppress the influence of small islands. Corresponding studies have been performed both theoretically and experimentally, and we can cite several identical examples for III–V [14] and Ge–Si [13, 60] systems. Such multilayered heterostructures with QDs are of practical importance in relation to arising new possibilities (for example, the electron coupling of clusters in the vertical direction and the formation of 3D arrays consisting of islands–clusters that are often referred to as "artificial atoms" [61, 62]).

3.3. The Sizes and Density of the Islands: Methods for Control

Figure 9 shows the characteristic sizes of GeSi clusters of the hut and dome types; it can be seen that the sizes increase with an increasing Si fraction in the GeSi solid solution (the data reported in [29, 42, 49, 63] were used). Theoretical dependence of the period of the surface undulation for the GeSi/Si(100) film is also shown; this undulation is a result of the elastic relaxation of the strained solid solution (this dependence was derived by Obayashi and Shintani [64]). As the fraction of Si increases, strains in a cluster decrease and the neces-

sary gain in energy due to elastic relaxation in the islands occurs for the larger island sizes. Studies of GeSi solid solutions with a large Si content, convenient for simulation experiments, make it possible to easily clarify the main laws of the island formation due to their relatively large sizes [49]. However, the practical interest of researchers focuses on the systems that contain the islands of about 10 nm or less in size (pure Ge on Si), which is primarily due to the optical properties of such systems. The density of islands is also very important because the response of the system to external effects is directly related to the number of islands and, correspondingly, to their density. Both of these parameters (the size and density) depend on the growth conditions such as the substrate temperature and the growth rate. A decrease in the growth temperature, as well as an increase in the Ge flux, causes the diffusion length of Ge adatoms at the substrate to decrease. Correspondingly, the collection region of adatoms for a single island decreases, the island size also decreases, whereas the island density increases. Abstreiter and coworkers [65] regularly varied the island density to 10^{10} cm^{-2} by decreasing the growth temperature to 550°C and increasing the Ge flux. Further decrease in the growth temperature to 300°C made it possible to appreciably increase the density of Ge nanoclusters to $\sim 3 \times 10^{11}$ cm^{-2} [66]. Peng and coworkers [67] used antimony as a surfactant that reduced the surface diffusion length of Ge adatoms and managed to obtain an island density of $\sim 5 \times 10^{11}$ cm^{-2} (the highest so far).

3.4. A Comparison of the Si {001} and {111} Surfaces

The vast majority of theoretical and experimental studies of formation of Ge islands have been devoted to these processes at the Si(001) surface because it is this surface that is most favorable for the formation of high-density coherent nanoislands. Nevertheless, the problem of the influence of the substrate-surface orientation on the island formation in a strained heteroepitaxial film remains topical; therefore, in this section, we attempt to dwell briefly on the special features that distinguish the Ge/Si(001) and Ge/Si(111) systems with respect to morphological instability.

When Ge is deposited on the Si(001) surface, the formation of the wetting layer is followed by the emergence of the coherent (without misfit dislocations) hut-shaped clusters (Fig. 5) and then by the dome-shaped clusters whose height significantly exceeds the critical thickness that corresponds to the onset of the introduction of the misfit dislocations [10]. These dislocations appear in islands whose height exceeds 50 nm [10] (the so-called superdome clusters [39]). Thus, in a Ge/Si(001) system, there is an extended domain of conditions for the existence of Ge 3D coherent islands. The 3D Ge islands formed at the Si(111) surface differ appreciably in shape and constitute triangular pyramids with flat tops (Fig. 10) and {113} lateral faces [48, 68–70];

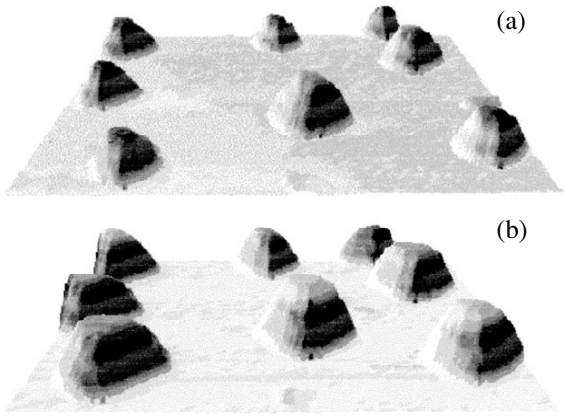

Fig. 10. A perspective STM image of typical Ge islands after the deposition of (a) 4.1 and (b) 6.8 Ge bilayers on the (111) surface of silicon. The image area is 330×330 nm^2. The average height of the islands in panel (b) is 8 nm. For details, see [68].

it is important that nanoislands contain the misfit dislocations even at the initial stages of island formation [71, 72].

As mentioned in Section 2, morphological instability of the strained-layer surface and the ultimate manifestation of this instability (the formation of the 3D coherent islands) develops if the gain in the free energy of the system due to elastic relaxation of stresses in the islands exceeds an addition to the surface energy due to an increase in the surface area and to the emergence of facets with a higher surface energy. We now compare the Ge/Si(001) and Ge/Si(111) systems taking into account the above considerations.

The facet closest to the (100) plane both for germanium [73, 74] and for silicon [75] is the (105) face and deviates by 11.3° from the (100) plane. According to the data reported elsewhere [76], this face consists of (100) terraces separated by steps. Formation of Ge–on–Si hut-shaped clusters faceted exactly by the {105} planes is due (according to the assumptions by Liu, Wu, and Lagally [77]) to an insignificant distinction between the surface energies of the {100} and {105} faces. On the other hand, the (113) face that facets the Ge 3D islands at the initial stage of their formation at the Si(111) plane [68] deviates from the basal plane by at least 29.5°. The surface energy (γ) of this face was determined experimentally for Si by Eaglesham and coworkers [78] and was found to be larger by a factor of 1.13 than the value of γ for the {111} plane. It was also experimentally demonstrated [78] that the step energy at the Si(111) surface is five times larger than that at the (001) surface, which is apparently the main factor conducive to the greater atomic smoothness of the (111) surface compared to the (001) surface and, correspondingly, to the greater morphological stability of this face. Barbezier and coworkers [72] also emphasize the deciding effect of the enhanced formation energy of the steps at the (111) surface compared to the

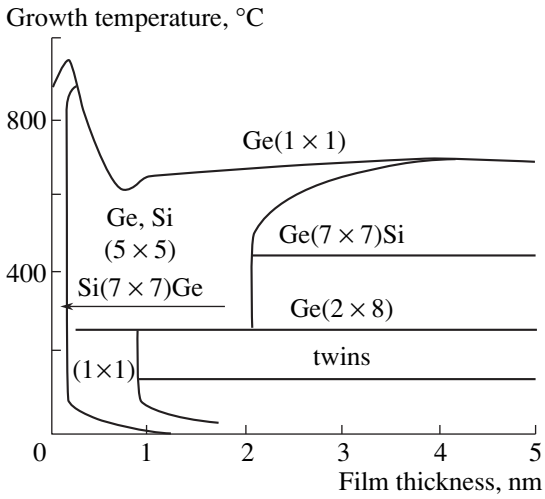

Fig. 11. Kinetic diagram of structural transitions at the film surface in the course of germanium heteroepitaxy onto the Si(111)–(7 × 7) surface.

(001) surface, which results in a higher morphological stability of the (111) face. Because of this, the 3D Ge islands at the Si(111) surface are shaped as truncated pyramids whose upper surface remains the same (111) plane and whose height is within 0.1–0.13 of their cross-sectional sizes [68]. We may assume that the clusters with such shapes are considerably less prone to stress relaxation due to elastic strains compared to the hut-shaped clusters at the (001) surfaces.

Thus, the Ge islands formed at the Si(111) surface are bound to gain less free energy due to elastic relaxation of stresses compared to the hut-shaped clusters at the (001) surface and should lose more surface energy due to a larger inclination angle of the nearest facet. We add to this comparison the fact that the (111) surface is the glide plane for dislocations, whereas the presence of an abrupt (111)–(113) step at the edge of a 3D island results in the so-called geometric enhancement of stresses, which reduces the energy barrier for the misfit-dislocation initiation. Correspondingly, such a shape of islands is conducive to the rapid onset of their plastic relaxation [79]. In our opinion, it is the combination of the aforementioned factors that gives rise to the fact that the existence domain for Ge 3D coherent islands in a Ge–Si(111) system is extremely narrow or is not present at all.

3.5. The Factors Influencing the Process of Ordering

It was mentioned above that the morphology of the surface at which the 3D islands are formed plays an important role and can be used as a controlling factor conducive to the ordering of the islands with respect to both their sizes and spatial distribution. The surface parameters may be controlled by the following methods:

(i) The use of the substrates that are tilted from the (001) surface and the various related methods for ordering the steps representing further the stencils for initiation of the islands [56, 80–86];

(ii) The use of surfactants that modify the surface characteristics (the surface energy and the diffusion length of adatoms) of both the substrate and the epilayer [67, 87–90];

(iii) The formation of microstressors at the substrate surface; these microstressors initiate the nucleation of islands at certain sites [91–93]; and

(iv) The use of lithography making it possible to form windows in the substrate; these windows restrict the region of collection of adatoms in the islands and separate the islands from each other [94, 95]. The photolithography-induced formation of facets that localize the initiation sites for the Ge islands [96, 97].

Each of these avenues of research are being developed; however, the studies are at the early stage. Because of this, we call the reader's attention to these avenues of research without analyzing them in detail.

3.6. The in situ Control

A strong dependence of the island parameters on the technological-process conditions makes it necessary to continuously control the growth surface of the substrate. A convenient method suitable for this purpose is the reflection high-energy electron diffraction (RHEED). As a typical example of a thorough study of the surface during heteroepitaxy, the RHEED was used [98] to plot the phase diagrams of structures that existed during epitaxy of Ge on the Si(111) and Si(001) substrates.

Figure 11 shows an example of such a diagram for the Si(111) surface. Two structures with a period multiple of 7 were observed during the epitaxy of Ge on Si(111). These structures are Si(111)–(7 × 7)Ge and Ge(111)–(7 × 7)Si. Here, the first chemical symbol indicates the material at whose surface a given superstructure was observed, whereas the second symbol indicates the material that stabilizes the given superstructure. The Si(111)–(7 × 7)Ge superstructure is formed at a high temperature if there is small amount of Ge at the Si surface. The highest temperature at which this superstructure was stable in the course of the film growth was 950°C. According to an estimate [98], the fluxes of adsorbing and desorbing Ge atoms are equal to each other at this temperature. As the temperature is increased further, the concentration of Ge atoms at the surface decreases rapidly.

After the critical thickness (corresponding to origination of the misfit dislocation) of the film has been attained, the Ge(111)–(7 × 7)Si superstructure is formed at the surface of Ge islands; this superstructure is stabilized by Si atoms that diffuse from the substrate. This conclusion is confirmed by the fact that the surface of the Ge film grown at a temperature below 350°C has

the Ge(111)–(2 × 8) superstructure, whereas the subsequent annealing of the film at 600–700°C gives rise to the Ge(111)–(7 × 7) superstructure. In addition to the aforementioned structures, the Ge(111)–(5 × 5) superstructure was also observed [99, 100]. The presence of the latter superstructure is related to the pseudomorphous state of the Ge film. After the pseudomorphism ceases to exist, this superstructure transforms either into Ge(111)–(7 × 7)Si or into Ge(111)–(2 × 8). The latter structure is characteristic of the atomically clean (111) surface of the bulk Ge. Consequently, the (5 × 5) structure is an indication that there are stresses in the film; relaxation of these may stimulate the formation of the islands.

Typically, the (2 × 1) and (2 × 8) superstructures are present at the surface during the growth of the Ge_xSi_{1-x} film on the Si(001) substrates. On the basis of the analysis of variations in the diffraction patterns in the course of the growth of Ge film on Si, we plotted [98] the phase diagram shown in Fig. 12. After the islands have been formed, the facets (Fig. 12) with the {105}, {118}, and {311} faces are observed [47, 101–103]. Correspondingly, in this case, the appearance of strands, which are related to the relevant crystal faces, at the RHEED pattern is an indication that the islands have been formed.

The shape of oscillations of a specular reflection in the electron-diffraction pattern observed during growth is also highly sensitive to morphological rearrangements at the surface of the growing film. This inherently high sensitivity of specular reflection to morphological features becomes even higher when the diffraction occurs under the conditions of surface resonance [104]. In these cases, the emergence of islands is accompanied by a drastic decrease in the specular-reflection intensity, which makes it possible to precisely determine the instant corresponding to the onset of the island formation.

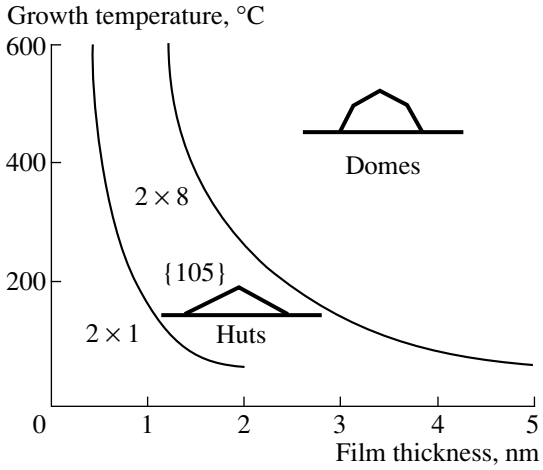

Fig. 12. Kinetic diagram of structural transitions at the film surface in the course of epitaxy onto the Si(001)–(2 × 1) substrate.

4. ELECTRONIC PROPERTIES OF SYSTEMS OF "ARTIFICIAL ATOMS"

Electronic properties of Ge–Si structures were studied by electron tunneling spectroscopy, capacitance spectroscopy, and conductance spectroscopy; in addition, the hopping conduction and the field effect were studied. The Ge–Si heterocombination belongs to heterostructures of the second type, in which the Ge islands constitute potential wells for holes. This fact governs the choice of the conduction type in the systems under consideration.

4.1. Electrical Properties

4.1.1. Electron tunneling spectroscopy. If the Fermi level in the emitter coincides with the allowed level of the charge carrier in a quantum well, a resonance enhancement of tunneling current should be observed. By changing the energy of the injected charge carrier by varying the voltage, one can obtain data on the energy spectrum of QDs. This spectroscopic method was first applied to the arrays of self-organized QDs in 1992 [6]. The structure studied included two parallel electrodes ($Ge_{0.3}Si_{0.7}$ layers doped heavily with boron) between which the Ge-nanocrystal layer [105] was confined, with potential barriers (Si interlayers) separating this layer from the electrodes. The dependence of differential conductance on the voltage is shown in Fig. 13. The upper panel corresponds to symmetric silicon barriers (both of them are 9 nm thick). The lower panel shows the conductance spectrum occurring in the situation when one of the barriers is thinner (the barrier thicknesses here are 9 and 6 nm); negative polarity of the voltage corresponds to the situation when a charge carrier (hole) first passes through the thin layer and then through the thick layer. In both cases, distinct oscillations of tunneling conductance of the structures are observed; these oscillations indicate that there exists a well-resolved discrete spectrum in the Ge islands. The oscillations in the vicinity of the zero bias are accompanied by the emergence of a region with negative differential conductance which is a characteristic feature of resonance tunneling. For the symmetric configuration of the barriers (see the upper panel in Fig. 13), the conductance oscillations are nearly symmetric with respect to the zero voltage and have a characteristic period of ~150 mV, which makes it possible to estimate the distance between the size-quantization levels at ~150/2 = 75 mV.

In the asymmetric structure, the conductance peaks are split into a series of oscillations with a smaller period in the region of negative biases. For this polarity of the voltage, accumulation of holes in the islands occurs as a result of a large difference between the coefficients of transit through the left and right barriers; thus, the processes of the charge-carrier Coulomb correlations caused by the carrier–carrier interaction

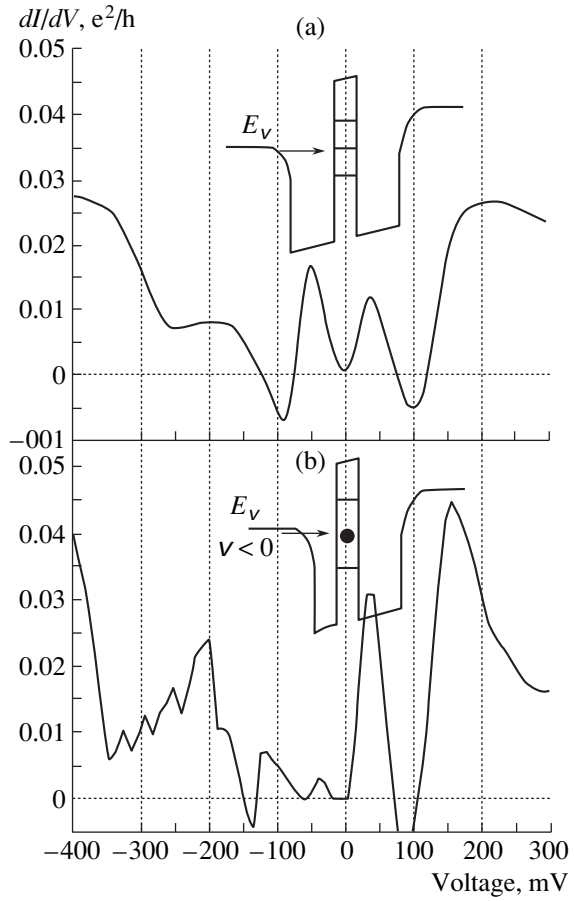

Fig. 13. Dependence of differential conductance of vertical two-barrier structures with Ge quantum dots for (a) a symmetric structure (the width of both Si barriers is 9 nm) and (b) an asymmetric structure (with barriers 6 and 9 nm wide).

become important. The Coulomb interaction removes the degeneracy of single-particle levels of size quantization since a hole overcomes the energy of electrostatic repulsion of charge carriers that are already present in the QD. Such an effect has been previously observed in the form of steplike current–voltage characteristics in tunneling transitions through metallic granules and has been named the "Coulomb staircase" [106]. The correlation energy of holes in the islands can be estimated from the distance between the conductance peaks at $E_C \approx 35$ meV in the ground state and at $E_C \approx 18$ meV in the first excited state.

4.1.2. Capacitance tunneling spectroscopy. The capacitance spectroscopy of QDs is based on the fact that the charge in zero-dimensional systems can change only discretely by a value of $\delta Q = eN$, where e is the elementary charge and N is the number of quantum dots in the sample [107]. The external voltage V_g at the gate electrode shifts the potential in the islands with respect to the Fermi level in the contact separated from the island-containing layer by a tunneling-transparent barrier and stimulates, either the capture of charge carriers from the contact by the QD levels, or the depopulation of these levels, depending on the polarity of V_g. If the Fermi level in the contact coincides with the bound-state energy in a QD, the differential capacitance $C(V_g) = dQ/dV_g$ is bound to feature a peak that is indicative of the presence of a discrete energy level. The total capacitance of the structure is a sum of two contributions: the first of these is due to the presence of a space-charge region in the material (in the case under consideration, this is silicon) that surrounds the islands, whereas the second contribution (C_{QD}) is related to the recharging of the QDs.

In the studied structures with the Schottky barrier, the effective layer thickness d_{eff} was varied [108]. The structures included the following sequence of layers beginning at the substrate: (i) the p^+-Si(100) substrate serving as the lower electrical contact; (ii) a $Si_{0.5}Ge_{0.2}$ layer having a thickness of $L = 10$ nm and ensuring an abrupt heteroboundary of the next Si tunneling barrier; (iii) a tunneling-transparent Si barrier ($p = 7 \times 10^{16}$ cm^{-3} and $L = 7$ nm); (iv) a layer containing the Ge nanocrystals; (v) a blocking Si layer ($p = 7 \times 10^{16}$ cm^{-3} and $L = 50$ nm); and (vi) an Al electrode controlling the occupancy of the islands and forming the Schottky barrier at the boundary with silicon. The area of the Al contact region was $\sim 8 \times 10^{-3}$ cm^2; a cylindrical mesastructure was etched off to a depth of about 5 μm according to the outline of this contact area.

The capacitance–voltage (C–V) characteristics of the structures without a Ge layer had a shape typical of a p-Si depletion layer (Fig. 14). In the case of $d_{eff} = 2$ monolayers (ML), a plateau appears in the C–V characteristics; this plateau is characteristic of a 2D charge-carrier gas. In the range of the effective Ge thicknesses of $8 \le d_{eff} \le 13$ ML, peaks appear in the C–V curves; the distance between these peaks, their width, and their position on the voltage scale (the energy scale) depends on d_{eff}: as d_{eff} increases, the peaks become narrower and their energy separation decreases. The energy distance between the levels corresponding to two capacitance peaks can be determined from the relationship $\Delta E = \Delta V_g b/L$ [109], where ΔV_g is the distance between the peaks in the C–V characteristic, b is the distance between a QD and the lower electrode, and L is the distance between the top and bottom electrodes. Calculations yield $\Delta E = 87$ ($d_{eff} = 8$ ML), 36 (for 10 ML), and 32 meV (13 ML) [108]. The value of $\Delta E = 36$ meV for the sample containing the amount of Ge that corresponds to $d_{eff} = 10$ ML is consistent with the recharging energy (E_C) of a QD in the ground state as was found in the experiments with resonance tunneling. Because of this, splitting of the peaks was attributed to the electrostatic Coulomb interaction.

The emergence of the capacitance oscillations is related to the formation of an array of Ge nanocrystals; this array is presumably rather uniform with respect to the island sizes, and the density of hole states in the array is a deltalike function of energy. For a large

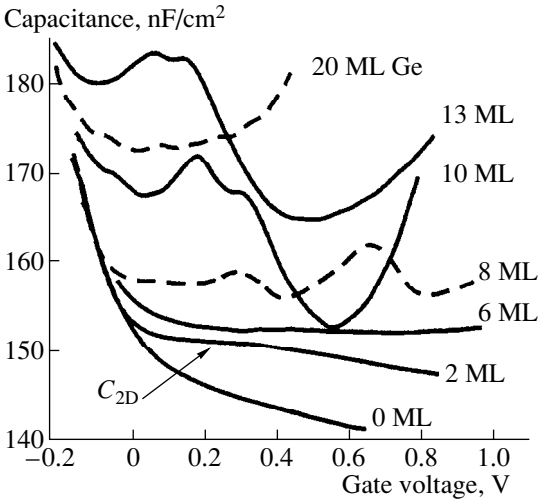

Fig. 14. The capacitance–voltage characteristics of Ge–Si(001) heterostructures with a different effective thickness (d_{eff}) of the Ge layer. The characteristics were measured at $T = 300$ K. Numbers at the curves indicate the value of d_{eff} measured in monolayers (ML).

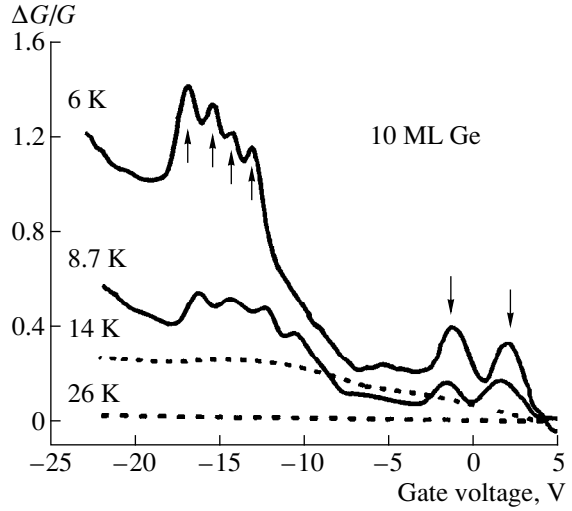

Fig. 15. Relative variation in the channel conductance of a field transistor that contains 10^9 quantum dots as a function of the gate voltage (the field effect) at different temperatures.

amount of deposited Ge (d_{eff} = 20 ML), plastic relaxation of elastic strains occurs and large (≈100 nm) islands with dislocations are formed. This is manifested by the disappearance of the capacitance peaks in the *C–V* characteristics. A large increase in the capacitance accompanied with a drastic increase in conductance for $d_{eff} > 20$ ML is apparently also related to the appearance of dislocations and the breakdown of the space-charge region.

The area under each peak (in the *C–V* characteristic) divided by the elementary charge was found to be almost exactly equal to the surface density of Ge islands ($2n_{QD} \approx 6 \times 10^{11}$ cm^{-2}). This means, first, that all Ge islands are involved in the process of recharging of the system and, second, that degeneracy in energy is removed owing to the Coulomb interaction.

Experimental verification of the Coulomb origin of splitting was found in the measurements of *C–V* characteristics for two layers of Ge islands with identical sizes [110]. In this case, the peak splitting caused by the Coulomb interaction increases.

4.1.3. The field effect. Variation in the conductance of MIS transistors, in which the conducting channel includes a layer of Ge nanocrystals, was found to be quite informative for studying the effects of electron correlations and quantum confinement [111]. Sequential population of the islands by charge carriers was accomplished by applying a voltage to the transistor gate. For the Ge-island density used (~3×10^{11} cm^{-2}), tunneling transitions between the states localized in different islands becomes important. The probability of a hole hopping between the QDs is defined by (I) the overlap of the wave functions for the occupied and empty states and (II) the occupancy of a given hole shell. If the relevant level is exactly half-occupied, the conductance is bound to be the largest and the activation energy for hops is bound to be defined by the electrostatic energy of interaction of a given hole with all charges in the nanocrystals. If the level is completely occupied, the charge carrier has to execute a transition to the excited states of the next shell. The activation energy increases by a value equal to the quantum-confinement energy, and the conductance decreases. As the occupancy of the excited state increases further, the activation energy required for the excitation of a charge carrier to the given level in other QDs decreases and again becomes a function of the electron–electron interaction, which brings about an increase in the contribution of the hopping conductivity, and so on. Thus, the hopping conductivity at a given temperature and also the activation energy for electrical conductivity are bound to oscillate with variations in the gate voltage, thus reflecting the structure of the spectrum of states. Such oscillations are inherent only in zero-dimensional systems where the electronic spectrum is discrete (atomlike).

Oscillations in the hopping conductivity under the conditions of the field effect were observed in MIS transistors that had a Ge layer with an effective thickness of more than 6 ML and contained up to 10^9 Ge islands [111]. A high-resistivity *n*-Si wafer was used as the substrate. In the low-temperature region ($T < 9$ K), oscillations were observed in the dependences of the channel conductance on the gate voltage; these oscillations corresponded to the occupation of the ground and excited states in a QD (Fig. 15).

In a MIS transistor with the QD layer formed on a silicon-on-insulator structure [separation by oxygen

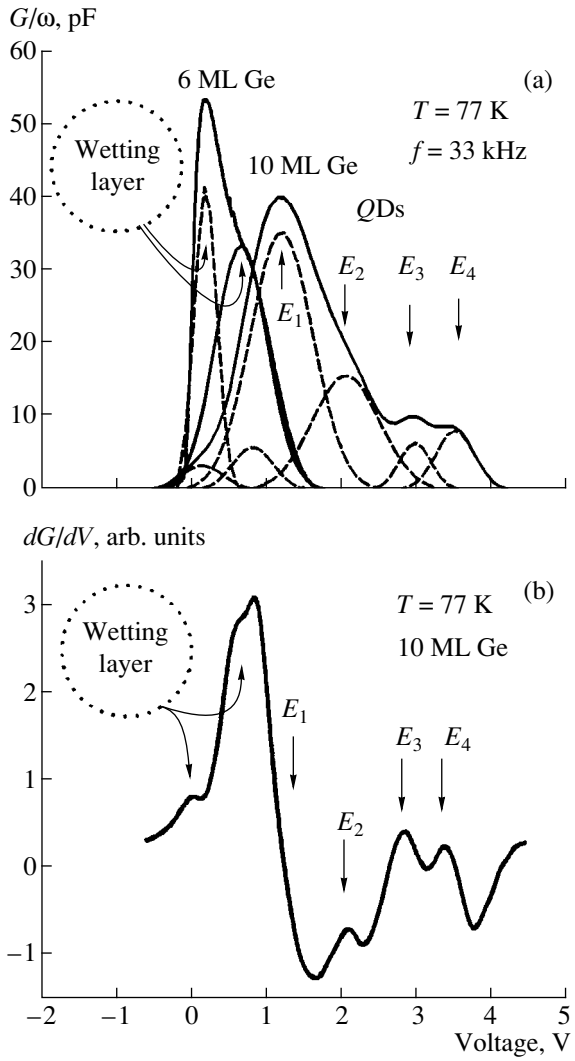

Fig. 16. (a) The admittance of the Schottky diode with quantum dots (10 ML of Ge) and with a continuous Ge layer (6 ML). The dashed lines represent the results of the decomposition of the experimental spectrum into Gaussians. The symbols E_1, E_2, E_3, and E_4 denote the response of discrete states in quantum dots. Figure 16b shows the derivative dG/dV.

implantation (SIMOX) technology was used] [112], the leakage currents through underlying Si layers were minimized; as a result, the conductance oscillations were observed at temperatures as high as ~150 K. The temperature dependence of conductance followed the Arrhenius law, which distinguishes the occurring processes from the resonance tunneling and substantiates the hopping mechanism of the charge transport over QDs.

4.1.4. Conductance spectroscopy. Measurements of admittance of the silicon Schottky barriers with a buried Ge-QD layer made it possible to gain additional information about the energy-spectrum structure of the QDs and the hole-state parameters [113]. In this case, the response of the QDs is equivalent to that of a capacitor with losses [114] and is characterized by the time constant $\tau = R_{QD}C_{QD}$. As the reverse bias increases in magnitude, the depletion layer penetrates deep into Si and, thus, brings about the depopulation of hole levels in a QD. Figure 16 shows the conductance (divided by the frequency of the periodic signal) as a function of the bias voltage for a structure with QDs (the sample with 10 ML of Ge) and a structure that contains only a wetting layer (6 ML of Ge). In the latter case, two peaks are observed at 0.1 and 0.6 V. Amplitudes of these peaks is frequency-independent in the range of 10–100 kHz; apparently, the peaks are related to the recharging of the wetting layer. For the sample with QDs, four additional peaks (denoted as E_1, E_2, E_3, and E_4 in Fig. 16) are observed. The temperature dependences of emission times made it possible to determine the activation energies (the depths of the corresponding levels): $E_1 = (201 \pm 7)$ meV, $E_2 = (228 \pm 7)$ meV, $E_3 = (267 \pm 12)$ meV, and $E_4 = (288 \pm 10)$ meV; the relevant capture cross sections were also determined (Fig. 17). The cross sections for the capture of holes by QDs increase with increasing level depths (Fig. 17) and exceed the known values for deep levels in Si by many orders of magnitude.

4.2. Optical Properties

Interest in the optical properties of QDs is caused by application-oriented considerations and by a number of advantages of such zero-dimensional objects compared to 2D QWs. Special features of QDs include, first, the possibility of controlling the spectral range of photoresponse by preliminarily populating the discrete states with the required transition energies; second, the presence of lateral quantization in zero-dimensional systems removes the forbiddenness of optical transitions polarized in the photodetector plane and, consequently, makes it possible to accomplish the absorption of light at a normal incidence of photons; and, third, an appreciable increase in the lifetime of charge carriers photogenerated in a QD due to the so-called "phonon bottleneck effect" [115].

4.2.1. Absorption in the infrared region of the spectrum. Absorption of light in the infrared (IR) region of the spectrum in Ge–Si multilayered heterostructures with self-organizing QDs has been studied previously [116, 117]. In both cases, the islands were ~40–50 nm broad at the base and were 2–4 nm in height. The density of the islands was ~10^8 cm^{-2}. The Ge islands were doped with boron [116] in order to populate the QD ground state with holes. A broad (~100 meV) line was observed in the absorption spectra within the wavelength range of 5–6 μm; the amplitude of this line decreased appreciably when the light with polarization perpendicular to the layer plane was used. This line was attributed to transitions between two lower levels of transverse quantization of heavy holes in a QD.

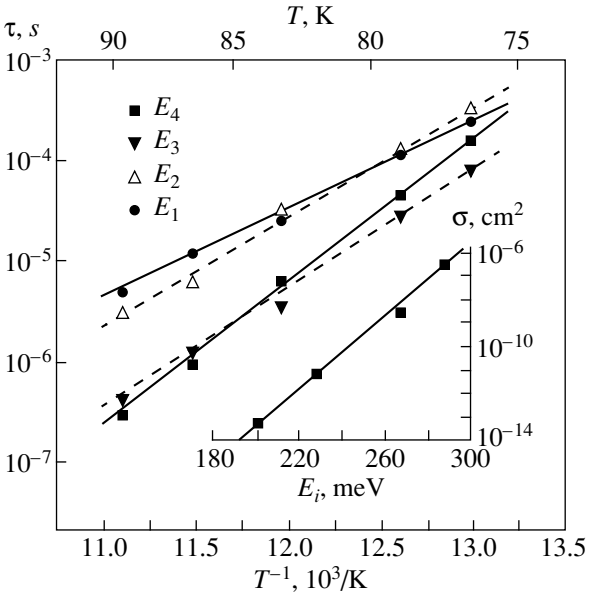

Fig. 17. Temperature dependence of the times of hole emission (τ) from excited state in quantum dots. Dependence of the cross section of the hole capture (σ) by the levels in quantum dots on the energy depth E_i of the levels is shown in the insert.

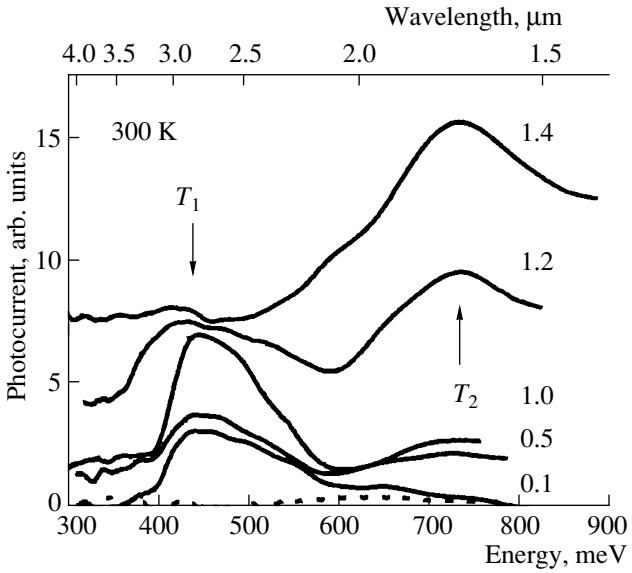

Fig. 18. The photocurrent spectra of a Si *p–i–n* diode with Ge quantum dots under a reverse bias indicated (in volts) at the corresponding curves. The dashed line demonstrates the absence of photoresponse in this range of photon energies in a structure with a continuous Ge layer (d_{eff} = 6 ML).

In order to activate optical transitions within an undoped QD, additional optical pumping was used [117]. The photoinduced absorption of light polarized parallel to the layer plane featured an asymmetric peak in the vicinity of 4.2 μm and was related to a transition of holes from the QD ground state to the valence-band delocalized states. The determined cross section for absorption [117] was unusually large (2×10^{-13} cm^2) and exceeded at least by an order of magnitude the known cross sections for photoionization of local centers in Si [118] and by three orders of magnitude the similar quantity for QDs in InAs–GaAs [119]. These data [117] indicate that a Ge–Si system has the potential to be used in IR photodetectors.

4.2.2. Photoconductivity. Observations of a photocurrent generated by photons with energy less than the band gap of silicon in Ge/Si heterostructures with QDs were first reported in [65, 120]. The possibility of developing a QD-containing photodetector tunable to the near- and medium-IR regions of the spectrum was demonstrated recently [66]. The photodetector was a silicon *p–i–n* diode, the base layer of which incorporated a 2D array of Ge nanoclusters. The average width of the QDs was 15 nm, and the height was 1.5 nm. The photocurrent spectra for various reverse-bias voltages are shown in Fig. 18. There was no photoresponse in the sample with continuous (d_{eff} = 6 ML) Ge film. In a structure with QDs, two peaks were observed at the wavelengths of 1.7 and 2.9 μm for photon energies lower than the energy corresponding to the fundamental-absorption edge in silicon (~1.12 eV). The heights of both peaks depended strongly on the reverse-bias voltage, with these dependences being correlated with each other. More specifically, as the magnitude of the bias was increased to 1.4 V, the photoresponse ceased to exist in the medium-IR region (at 2.9 μm, line T_1) and a signal in the near-IR region of the spectrum emerged (at 1.7 μm, line T_2). The photon energy corresponding to the peak of line T_1 (430 meV) coincides with the energy depth of the ground state of a hole in a QD [121]. Therefore, line T_1 was related to a transition of a hole from the ground state localized in a QD to delocalized states in the valence band. As the magnitude of the reverse bias increases, the hole levels in a QD are filled with electrons. In the region of voltages in the vicinity of 1.4 V, a QD becomes completely depleted of holes and transition T_1 turns out to be "forbidden." Starting from this moment, the band-to-band transitions of electrons between the valence and conduction bands become possible (process T_2). Since the system under consideration belongs to heterostructures of the second type (holes are localized in Ge regions, whereas these regions constitute potential barriers for electrons [122]), the band-to-band optical transition is indirect in the coordinate space and is accompanied with the transfer of electrons from Ge to Si. The energy of transition should be governed by the difference between the band gap of Si (1.12 eV) and the energy of the hole state in a Ge QD (0.43 eV); i.e., it should be equal to 700 meV, which is consistent with the experimental position of line T_2 (≈730 meV).

4.2.3. Photoluminescence. Conventionally, measurements of photoluminescence (PL) spectra are used to check the formation of the self-organizing QD lay-

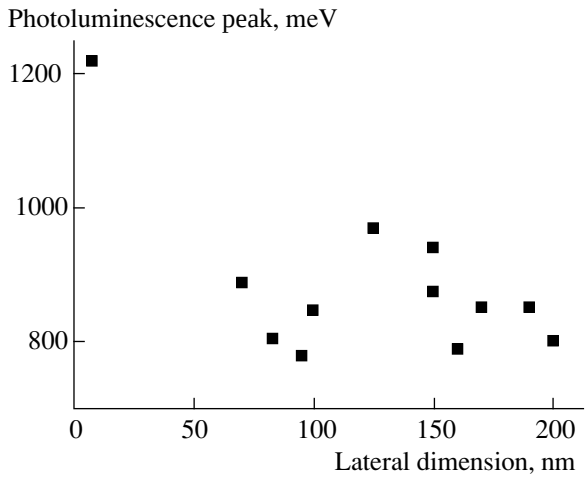

Fig. 19. The energy of the photoluminescence peak as a function of the lateral dimension of germanium islands in silicon.

ers; these measurements make it possible to determine the energies of the ground and excited states in a QD. For an InAs/GaAs system, the PL data were summarized and analyzed in [123]. In particular, it was shown [123] that the photon energy of the emission from QDs is controlled by the effective thickness of the deposited InAs layer and, as a result, by the QD size. The results of PL measurements as an illustration of the nucleation and evolution of QDs are also reported in many publications devoted to the epitaxy of Ge–Si structures. The appearance of a band in the vicinity of 800–900 meV in the PL spectra is related to the formation of Ge islands [13, 117, 120, 122–130]. The width of this band is tens of millielectronvolts; only once [124] were narrow (~2–10 meV) PL lines observed and attributed to the formation of an array of QDs that were uniform (to ~3%) in size. Nevertheless, in our opinion, the interpretation of the PL spectra for Ge–Si structures is somewhat contradictory. Figure 19 shows the position of a PL peak related previously to Ge islands as a function of the lateral size of nanoclusters. Here, we used the data reported in [13, 117, 120, 122–130]. In contrast with an InAs/GaAs system, a distinct dependence of the radiative-transition energies on the QD size is not observed; at the same time, it should be reasonable to expect that, as the QD size increases, the PL peak would shift to lower energies in the spectrum as a result of a decrease in the quantum-confinement energy in the islands. In addition, the observation of an emission with energy larger than the band gap of silicon [125] (the leftmost point in Fig. 19) seems surprising. All these circumstances have no generally accepted satisfactory explanation at present and will stimulate further thorough studies of mechanisms for PL in Ge–Si structures.

5. CONCLUSION

In this review, we analyzed scientific publications worldwide and noted the growing interest of scientists and technologists in the problems of the production and the application of nanostructures that are based on silicon and germanium and consist of Ge clusters of nanometer-scale size (quantum dots) embedded in the Si matrix. Elastic strain in epilayers and 3D Ge islands on Si is a key factor that not only initiates the morphological transition from a planar film to an island-containing film (the Stranski–Krastanov mechanism) but also influences the subsequent stages of evolution of the islands, including their shape, size, and spatial distribution. In many cases, this factor modifies substantially the classical stages of the phase-formation mechanisms and their sequence to the point of a quasi-equilibrium coexistence of 3D Ge nanoislands at the surface of Si substrate. In the considered systems of nanoclusters, we separated out various types of ordering: ordering with respect to the cluster shape, to its size, to the distance between islands and their mutual arrangement, and also ordering in the vertical direction (in the sequentially formed multilayered heterostructures with quantum dots). The method for enhancing the degree of ordering in nanostructures with arrays of quantum dots and attaining ultimately small sizes and a large density of distribution over the surface area was discussed.

In this review, we also cite the published data on the absorption of light in multilayered Ge–Si systems; these data are indicative of an anomalously large cross section of intraband absorption, which makes the class of nanostructures under consideration promising for the development of the IR-region photodetectors. Applying the tunneling, capacitance, and conductance spectroscopies, and also the field effect to the transistor structures that contained no less than 10^9 Ge nanoclusters, we observed well-resolved peaks related to a single-electron capture of up to six holes by each quantum dot. The main factors controlling the spectrum of states are the quantum confinement and Coulomb interaction between charge carriers. A new factor arising in the QD array and distinguishing it from the situation with a single QD is the Coulomb correlation between the islands.

Studies of the electrical and optical characteristics of arrays of Ge islands in Si make it possible to draw a conclusion regarding the formation of arrays of "artificial atoms" that feature a discrete energy spectrum; the latter is observed up to room temperature.

ACKNOWLEDGMENTS

This work was supported by the Russian Foundation for Basic Research (project nos. 00-02-17461, 00-02-17638, and 00-15-96806) and the Program of the Ministry of Science of Russian Federation "The Physics of Solid-State Nanostructures."

REFERENCES

1. R.A. Mezger, Compd. Semicond. **1**, 21 (1995).
2. U. Konig, Phys. Scr., T **68**, 90 (1996).
3. R. A. Soref, Thin Solid Films **294**, 325 (1997).
4. T. Tashiro, T. Tatsumi, M. Sugiyama, *et al.*, IEEE Trans. Electron Devices **44**, 545 (1997).
5. D. J. Paul, Thin Solid Films **321**, 172 (1998).
6. A. I. Yakimov, V. A. Markov, A. V. Dvurechenskiĭ, and O. P. Pchelyakov, Philos. Mag. B **65**, 701 (1992).
7. D. Leonard, M. Krishnamurthy, C.M. Reaves, *et al.*, Appl. Phys. Lett. **63**, 3203 (1993); D. Leonard, K. Pond, and P.M. Petroff, Phys. Rev. B **50**, 11687 (1994).
8. J.-M. Marzin, J.-M. Gerard, A. Izrael, and D. Barrier, Phys. Rev. Lett. **73**, 716 (1994).
9. L. N. Aleksandrov, R. N. Lovyagin, O. P. Pchelyakov, and S. I. Stenin, J. Cryst. Growth **24/25**, 298 (1974).
10. D. J. Eaglesham and M. Cerullo, Phys. Rev. Lett. **64**, 1943 (1990).
11. S. Guha, A. Madhukar, and K. C. Rajkumar, Appl. Phys. Lett. **57**, 2110 (1990).
12. R. Nötzel, Semicond. Sci. Technol. **11**, 1365 (1996).
13. F. Liu and M. G. Lagally, Surf. Sci. **386**, 169 (1997).
14. N. N. Ledentsov, V. M. Ustinov, V. A. Shchukin, *et al.*, Fiz. Tekh. Poluprovodn. (St. Petersburg) **32**, 385 (1998) [Semiconductors **32**, 343 (1998)].
15. P. Müller and R. Kern, J. Cryst. Growth **193**, 257 (1998).
16. A. A. Chernov, E. I. Givargizov, and Kh. S. Bagdasarov, in *Modern Crystallography*, Vol. 3: *Crystal Growth* (Nauka, Moscow, 1980; Springer-Verlag, Berlin, 1984).
17. F. Liu and M. G. Lagally, Phys. Rev. Lett. **76**, 3156 (1996).
18. R. J. Asaro and W. A. Tiller, Metall. Trans. **3**, 789 (1972).
19. M. A. Grinfel'd, Dokl. Akad. Nauk SSSR **290**, 1358 (1986) [Sov. Phys. Dokl. **31**, 831 (1986)].
20. W. Dorsch, H. P. Strunk, H. Wawra, *et al.*, Appl. Phys. Lett. **72**, 179 (1998).
21. Yu. B. Bolkhovityanov, V. I. Yudaev, and A. K. Gutakovsky, Thin Solid Films **137**, 111 (1986).
22. S. A. Kukushkin and A. V. Osipov, Usp. Fiz. Nauk **168**, 1083 (1998).
23. I. M. Lifshitz and V. V. Slyozov, J. Phys. Chem. Solids **19**, 35 (1961).
24. B. K. Chakraverty, J. Phys. Chem. Solids **28**, 2401 (1967).
25. M. C. Bartelt and J. W. Evans, Phys. Rev. B **46**, 12675 (1992).
26. N. C. Bartelt, W. Theis, and R. M. Tromp, Phys. Rev. B **54**, 11741 (1996).
27. I. Goldfarb, P. T. Hayden, J. H. G. Owen, and G. A. D. Briggs, Phys. Rev. Lett. **78**, 3959 (1997); Phys. Rev. B **56**, 10459 (1997).
28. B. A. Joyce, D. D. Vvedensky, A. R. Avery, *et al.*, Appl. Surf. Sci. **130–132**, 357 (1998).
29. T. I. Kamins, G. Medeiros-Ribeiro, D. A. A. Ohlberg, and R. Stanley Williams, J. Appl. Phys. **85**, 1159 (1999).
30. A. R. Avery, H. T. Dobbs, D. M. Holmes, *et al.*, Phys. Rev. Lett. **79**, 3938 (1997).
31. J. Drucker, Phys. Rev. B **48**, 18203 (1993).
32. Y. Chen and J. Washburn, Phys. Rev. Lett. **77**, 4046 (1996).
33. D. E. Jesson, G. Chen, K. M. Chen, and S. J. Pennycook, Phys. Rev. Lett. **80**, 5156 (1998).
34. M. Kästner and B. Voigtländer, Phys. Rev. Lett. **82**, 2745 (1999).
35. T. I. Kamins, E. C. Carr, R. S. Williams, and S. J. Rosner, J. Appl. Phys. **81**, 211 (1997).
36. G. Medeiros-Ribeiro, A. M. Bratkovski, T. I. Kamins, *et al.*, Science **279**, 353 (1998).
37. G. Medeiros-Ribeiro, T. I. Kamins, D. A. A. Ohlberg, and R. S. Williams, Phys. Rev. B **58**, 3533 (1998).
38. T. I. Kamins, G. Medeiros-Ribeiro, D. A. A. Ohlberg, and R. S. Williams, Appl. Phys. A: Solids Surf. **67**, 727 (1998).
39. R. S. Williams, G. Medeiros-Ribeiro, T. I. Kamins, and D. A. A. Ohlberg, J. Phys. Chem. B **102**, 9605 (1998).
40. T. I. Kamins, G. A. D. Briggs, and R. Stanley Williams, Appl. Phys. Lett. **73**, 1862 (1998).
41. F. M. Ross, J. Tersoff, and R. M. Tromp, Phys. Rev. Lett. **80**, 984 (1998); Microsc. Microanal. **4**, 254 (1998).
42. N. V. Vostokov, S. A. Gusev, I. V. Dolgov, *et al.*, Fiz. Tekh. Poluprovodn. (St. Petersburg) **34**, 8 (2000) [Semiconductors **34**, 6 (2000)].
43. C.-H. Chiu, Appl. Phys. Lett. **75**, 3473 (1999).
44. V. A. Shchukin and D. Bimberg, Appl. Phys. A: Solids Surf. **67**, 687 (1998); Rev. Mod. Phys. **71**, 1125 (1999).
45. P. Müller and R. Kern, J. Cryst. Growth **193**, 257 (1998).
46. J. A. Floro, V. B. Sinclair, E. Chason, *et al.*, Phys. Rev. Lett. **84**, 701 (2000).
47. Y.-W. Mo, D. E. Savage, B. S. Swartzentruber, and M. G. Lagally, Phys. Rev. Lett. **65**, 1020 (1990).
48. S. M. Pintus, S. M. Stenin, A. I. Toropov, *et al.*, Thin Solid Films **151**, 275 (1998).
49. J. A. Floro, E. Chason, L. B. Freund, *et al.*, Phys. Rev. B **59**, 1990 (1999).
50. F. K. LeGoues, M. C. Reuter, J. Tersoff, *et al.*, Phys. Rev. Lett. **73**, 300 (1994).
51. H. T. Johnson and L. B. Freund, J. Appl. Phys. **81**, 6081 (1997).
52. V. A. Markov, A. I. Nikiforov, and O. P. Pchelyakov, J. Cryst. Growth **175/176**, 736 (1997).
53. Z. Jiang, H. Zhu, F. Lu, *et al.*, Thin Solid Films **321**, 60 (1998).
54. V. A. Markov, O. P. Pchelyakov, L. V. Sokolov, *et al.*, Surf. Sci. **250**, 229 (1991).
55. Y. Kim, B. D. Min, and E. K. Kim, J. Appl. Phys. **85**, 2140 (1999).
56. J. Zhu, K. Brunner, and G. Abstreiter, Appl. Phys. Lett. **73**, 620 (1998).
57. J. Johansson and W. Seifert, Appl. Surf. Sci. **148**, 86 (1999).
58. O. P. Pchelyakov, I. G. Neisvestnyi, and Z. Sh. Yanovitskaya, Phys. Low-Dimens. Struct. **10/11**, 389 (1995).

59. J. A. Floro, E. Chason, M. B. Sinclair, *et al.*, Appl. Phys. Lett. **73**, 951 (1998).
60. H. Omi and T. Ogino, Appl. Surf. Sci. **130–132**, 781 (1998).
61. G. Springholz, V. Holy, M. Pinczolits, and G. Bauer, Science **282**, 734 (1998).
62. Y. W. Zhang, S. J. Xu, and C.-H. Chiu, Appl. Phys. Lett. **74**, 1809 (1999).
63. F. M. Ross, R. M. Tromp, and M. C. Reuter, Science **286**, 1931 (1999).
64. Y. Obayashi and K. Shintani, J. Appl. Phys. **84**, 3141 (1998).
65. G. Abstreiter, P. Schittenhelm, C. Engel, *et al.*, Semicond. Sci. Technol. **11**, 1521 (1996).
66. A. I. Yakimov, A. V. Dvurechenskiĭ, Yu. Yu. Proskuryakov, *et al.*, Appl. Phys. Lett. **75**, 1413 (1999).
67. C. S. Peng, Q. Huang, W. Q. Cheng, *et al.*, Appl. Phys. Lett. **72**, 2541 (1998).
68. B. Voigtländer and A. Zinner, Appl. Phys. Lett. **63**, 3055 (1993).
69. P. W. Deelman, L. J. Schawalter, and T. Thundat, J. Vac. Sci. Technol. A **15**, 930 (1997).
70. A. Shklyaev, M. Shibata, and M. Ichikawa, Surf. Sci. **416**, 192 (1998).
71. L. N. Aleksandrov, R. N. Lovyagin, O. P. Pchelyakov, and S. I. Stenin, in *Growth and Doping of Semiconductor Crystals and Films* (Nauka, Novosibirsk, 1977), Part II, p. 139.
72. I. Berbezier, B. Gallas, A. Ronda, and J. Derrien, Surf. Sci. **412/413**, 415 (1998).
73. B. Z. Ol'shanetskiĭ, V. I. Mashanov, and A. I. Nikiforov, Fiz. Tverd. Tela (Leningrad) **23**, 2567 (1981) [Sov. Phys. Solid State **23**, 1505 (1981)].
74. Z. Gai, R. G. Zhao, H. Ji, *et al.*, Phys. Rev. B **56**, 12308 (1997).
75. B. Z. Olshanetsky and V. I. Mashanov, Surf. Sci. **111**, 414 (1981).
76. B. Z. Olshanetsky, A. E. Solovyov, A. E. Dolbak, and A. A. Maslov, Surf. Sci. **306**, 327 (1994).
77. F. Liu, F. Wu, and M. G. Lagally, Chem. Rev. **97**, 1045 (1997).
78. D. J. Eaglesham, A. E. White, L. C. Feldman, *et al.*, Phys. Rev. Lett. **70**, 1643 (1993).
79. J. Walz, A. Greuer, G. Wedler, *et al.*, Appl. Phys. Lett. **73**, 2579 (1998).
80. M. Abdallah, I. Berbezier, P. Dawson, *et al.*, Thin Solid Films **336**, 256 (1998).
81. J. Zhu, K. Brunner, and G. Abstreiter, Appl. Phys. Lett. **72**, 424 (1998).
82. K. Sakamoto, H. Matsuhata, M. O. Tanner, *et al.*, Thin Solid Films **321**, 55 (1998).
83. H. Omi and T. Ogino, Appl. Surf. Sci. **130–132**, 781 (1998).
84. H. Omi and T. Ogino, Phys. Rev. B **59**, 7521 (1999).
85. D. Martou, P. Gentile, and N. Magnea, J. Cryst. Growth **201/202**, 101 (1999).
86. Y. Homma, P. Finnie, T. Ogino, *et al.*, J. Appl. Phys. **86**, 3083 (1999).
87. C. W. Oh, E. Kim, and Y. H. Lee, Phys. Rev. Lett. **76**, 776 (1996).
88. A. Nagashima, T. Kimura, and J. Yoshino, Appl. Surf. Sci. **130–132**, 248 (1998).
89. T. Tezuka and N. Sugiyama, J. Appl. Phys. **83**, 5239 (1998).
90. V. Le Thanh, Thin Solid Films **321**, 98 (1998).
91. X. Deng and M. Krishnamurthy, Phys. Rev. Lett. **81**, 1473 (1998).
92. O. G. Schmidt, C. Lange, K. Eberl, *et al.*, Thin Solid Films **321**, 70 (1998).
93. O. Leifeld, R. Hartmann, E. Müller, *et al.*, Nanotechnology **10**, 122 (1999).
94. E. S. Kim, N. Usami, and Y. Shiraki, Appl. Phys. Lett. **72**, 1617 (1998).
95. A. A. Shklyaev, M. Shibata, and M. Ichikawa, Appl. Phys. Lett. **72**, 320 (1998).
96. T. I. Kamins and R. S. Williams, Appl. Phys. Lett. **71**, 1201 (1997).
97. T. I. Kamins, R. S. Williams, and D. P. Basile, Nanotechnology **10**, 117 (1999).
98. O. P. Pchelyakov, V. A. Markov, A. I. Nikiforov, and L. V. Sokolov, Thin Solid Films **306**, 299 (1997).
99. L. V. Sokolov, M. A. Lamin, O. P. Pchelyakov, *et al.*, Poverkhnost' **9**, 75 (1985).
100. M. A. Lamin, O. P. Pchelyakov, L. V. Sokolov, *et al.*, Surf. Sci. **207**, 418 (1989).
101. N. Ohshima, Y. Koide, S. Zaima, and Y. Yasuda, J. Cryst. Growth **115**, 106 (1991).
102. Y. Koide, A. Furukawa, S. Zaima, and Y. Yasuda, J. Cryst. Growth **115**, 365 (1991).
103. C. Tatsuyama, T. Terasaki, H. Obata, *et al.*, J. Cryst. Growth **115**, 112 (1991).
104. K. Reginski, M. A. Lamin, V. I. Mashanov, *et al.*, Surf. Sci. **327**, 93 (1995).
105. A. I. Yakimov, V. A. Markov, A. V. Dvurechenskiĭ, and O. P. Pchelyakov, J. Phys.: Condens. Matter **6**, 2573 (1994).
106. U. Meirav and E. B. Foxman, Semicond. Sci. Technol. **10**, 255 (1995).
107. R. C. Ashoori, H. L. Stormer, J. S. Weiner, *et al.*, Phys. Rev. Lett. **68**, 3088 (1992).
108. A. I. Yakimov, A. V. Dvurechenskiĭ, A. I. Nikiforov, and O. P. Pchelyakov, Pis'ma Zh. Éksp. Teor. Fiz. **68**, 125 (1998) [JETP Lett. **68**, 135 (1998)].
109. G. Medeiros-Ribeiro, D. Leonard, and P. M. Petroff, Appl. Phys. Lett. **66**, 1767 (1995).
110. A. I. Yakimov, A. V. Dvurechenskiĭ, A. I. Nikiforov, and O. P. Pchelyakov, Thin Solid Films **336**, 332 (1998).
111. A. I. Yakimov, C. J. Adkins, R. Boucher, *et al.*, Phys. Rev. B **59**, 12598 (1999).
112. A. I. Yakimov, A. V. Dvurechenskiĭ, V. V. Kirienko, *et al.*, J. Phys.: Condens. Matter **11**, 9715 (1999).
113. A. I. Yakimov, A. V. Dvurechenskiĭ, A. I. Nikiforov, and O. P. Pchelyakov, Phys. Low-Dimens. Struct. **3/4**, 99 (1999).
114. S. Anand, N. Carlsson, M.-E. Pistol, *et al.*, J. Appl. Phys. **84**, 3747 (1998).

115. M. Sugawara, K. Mukai, and H. Shoji, Appl. Phys. Lett. **71**, 2791 (1997).
116. J. L. Liu, W. G. Wu, A. Balandin, *et al.*, Appl. Phys. Lett. **74**, 185 (1999).
117. P. Boucaud, V. Le Thanh, S. Sauvage, *et al.*, Appl. Phys. Lett. **74**, 401 (1999).
118. D. K. Schreder, in *Charge-Coupled Devices*, Ed. by D. Barbe (Springer-Verlag, Heidelberg, 1980; Mir, Moscow, 1982).
119. S. Sauvage, P. Boucaud, J.-M. Gerard, and V. Thierry-Mieg, Phys. Rev. B **58**, 10562 (1998).
120. P. Schittenhelm, C. Engel, F. Findeis, *et al.*, J. Vac. Sci. Technol. B **16**, 1575 (1998).
121. S. K. Zhang, H. J. Zhu, F. Lu, *et al.*, Phys. Rev. Lett. **80**, 3340 (1998).
122. V. Ya. Aleshkin, N. A. Bukin, N. G. Kalugin, *et al.*, Pis'ma Zh. Éksp. Teor. Fiz. **67**, 46 (1998) [JETP Lett. **67**, 48 (1998)].
123. M. Grassi Alessi, M. Capizzi, A. S. Bhatti, *et al.*, Phys. Rev. B **59**, 7620 (1999).
124. X. Wang, Z. Jiang, H. Zhu, *et al.*, Appl. Phys. Lett. **71**, 3543 (1997).
125. C. S. Peng, Q. Huang, Y. H. Zhang, *et al.*, Thin Solid Films **323**, 174 (1998).
126. P. Boucaud, V. Le Thanh, S. Sauvage, *et al.*, Thin Solid Films **336**, 240 (1998).
127. E. S. Kim, N. Usami, and Y. Shiraki, Appl. Phys. Lett. **72**, 1617 (1998).
128. E. Mateeva, P. Sutter, and M. G. Lagally, Appl. Phys. Lett. **74**, 567 (1999).
129. E. Palange, G. Capellini, L. Di Gaspare, and F. Evangelisti, Appl. Phys. Lett. **68**, 2982 (1996).
130. R. Apetz, L. Vescan, A. Hartmann, *et al.*, Appl. Phys. Lett. **66**, 445 (1995).

Translated by A. Spitsyn